On-Line Condition Monitoring for Diagnosis and Prognosis of Insulation Degradation of Inverter-fed Machines

Igor Tsyokhla, *Member, IEEE,* Antonio Griffo, *Member, IEEE,*
and Jiabin Wang, *Senior Member, IEEE*

***Abstract*— Real-time winding insulation condition monitoring is becoming an important research topic in response to increase in high availability and reliability demands in modern drives. In this paper, a novel method is proposed to monitor ground-wall insulation of low voltage inverter-fed machines based on a multi-frequency measurement of equivalent insulation ground-wall capacitance and dissipation factor. The monitoring is applied to four machine stator samples subjected to accelerated aging until failure. Insulation degradation is continuously tracked via the capacitance and dissipation parameters. A link between ground-wall insulation capacitance and final lifetime is established. The relationship between capacitance progression and its value at final machine failure is used to develop a method for prognosis of the final failure time.**

***Index Terms*— Condition Monitoring, Dielectric Constant, Fault Diagnosis, Insulation, Preventative Maintenance, Prognostics and Health.**

I. Introduction

ELECTRICAL machine reliability and availability are two key requirements in many safety critical applications as well as applications where downtime caused by faults or maintenance results in significant loss of revenues. In response to the requirements of availability and fault detection, there has been a recently upsurge of interest in real-time on-line condition monitoring of machine health during its lifetime. The final goal is to replace costly periodic routine manual maintenance with condition-based maintenance performed based on the predicted remaining useful lifetime (RUL) estimated by on-line monitoring equipment.

Many types of faults can result in the stoppage of machine operation. A number of industrial surveys [1], [2] consistently identify bearing failure as the most prevalent cause, followed by failure of the winding insulation. It is relatively difficult to replace failed windings on a machine, and is often not considered economical unless for large plant. Therefore, when bearing maintenance and replacement is made routinely, the effective life of a machine is constrained by the winding failure.

Winding insulation is subject to four stress factors over its lifetime: material decomposition over time the rate of which depends on operating temperature, electrically induced damage, contamination from the surrounding environment and mechanical damage due thermal cycling, opposing Lorentz force and vibration. Simulation shows that small machines can be subject to significant mechanical stress [3], however little experimental evidence on the practical implication of these is published in literature. Electrical damage to insulation has been the subject of extensive studies, especially in medium and high voltage machines where partial discharge (PD) is a significant failure contributor. Although standards exist that aim to eliminate occurrence of PD with appropriate design measures in small machines [4], it has recently been found that fast switching transients (high dV/dt) in inverter-driven machines can cause significant PD in practice [5]. Environmental ingress of moisture and other contaminants can also lead to rapid failure of the machine. This paper aims at studying winding health over machine lifetime; therefore, thermal ageing of the winding insulation has been selected as the dominant long-term ageing factor. Mechanical and environmental factors have been eliminated from the experiment by removing the rotor, operating at constant temperature in a closed environmental chamber therefore removing almost all vibration and differential stress due to different coefficients of thermal expansion. With constant inverter bus and machine line voltage electrical stress is also treated as a constant.

In [6] it was recognized that the degradation of insulation material could be treated as a chemical reaction. To predict the rate of reaction, the Arrhenius equation can then be used. The principle of using temperature as the dominant ageing factor has since been adopted in machine testing standards [7] and machine design. Insulation lifetime based on temperature is predicted using (1), derived from the Arrhenius equation, where the predicted lifetime L is calculated in response to

Manuscript received April 21, 2018; revised July 25, 2018; accepted November 25, 2018. This work was supported by Engineering and Physical Sciences Research Council-EPSRC Grants EP/S00081X/1, EP/P010350/1 and EP/K034987/1.

A. Griffo and J. Wang are with the Department of Electronic and Electrical Engineering, The University of Sheffield, Sheffield, U.K., I. Tsyokhla is with Sphere Fluidics Ltd., Cambridge, U.K. (e-mail: A.Griffo@sheffield.ac.uk).

temperature T (in Kelvin) based on the initial lifetime L_0 and temperature rating class T_0.

$$L = L_0 e^{\frac{E_a}{R}\left(\frac{1}{T}-\frac{1}{T_0}\right)} \quad (1)$$

The activation energy E_a can be measured using differential scanning calorimetry as in [8] or more commonly by using accelerated ageing tests on insulation material samples as described in IEEE Std. 98 [9]. The methodology in IEEE Std. 98 is adopted in Section IV to age four stator samples at different rates and observe the material property changes in the ground-wall insulation using the monitoring equipment.

It has been demonstrated that progressive degradation affects the dielectric properties of the insulation material [10], [11]. This is routinely used in standard tests for machine insulation health such as measurement of insulation resistance, dissipation factor (DF, $\tan\delta$), leakage current and polarization index. However, these tests can only be performed offline, requiring temporary interruption of machine operation with consequent loss of availability. The observation that changes in dielectric properties occur due to ageing has led to the development of a number of insulation health monitoring methods suitable for online application [12]-[18]. These methods, however, have not been practically demonstrated yet during long-term ageing in inverter-driven machines. This paper describes a practical method suitable for ground-wall (GW) insulation monitoring and demonstrates its effectiveness in detecting gradual ageing over a long-term degradation test. The method, based on the spectral analysis of the common-mode impedance of the GW insulation, exploits the intrinsic common-mode excitation due to space-vector pulse-width modulation (SV-PWM) in standard two-level converters. Through lifetime ageing of four machine samples, it is demonstrated that the equivalent capacitance C_{eq} is a reliable indicator of ageing and a simple prognostic method based on C_{eq} is proposed for the estimation of the RUL.

II. Ground-Wall Impedance

In low voltage random wound machines, insulation is commonly made of organic insulating material that degrades over time. The voltage withstand capabilities and mechanical strength decrease over time [19], accelerated primarily by heat induced thermal degradation. Organic insulation consists of long polymer chains of the polymer element. Common polymers used in insulation are polyester, polyurethane, polyimide and others. Evidence from transformer insulation testing shows that longer chains exhibit stronger mechanical and electrical properties [20]. Over time, the chains break up and reform, exhibiting changed properties depending on the mechanism of degradation [21].

Off-line testing used in capacitance and dissipation factor testing consider the ground wall as a parallel plate capacitor, with the insulating dielectric between the plates formed by the winding copper and stator iron as in Fig. 1. It was shown in [18] that the model used in off-line testing is only applicable at a single test frequency. In order to use data measured at multiple frequencies and return a result comparable with off-line measurement practice, a novel way to interpret multi-frequency data is presented.

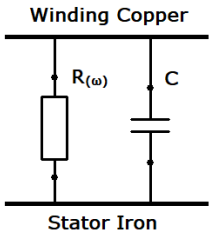

Fig. 1. Ground-wall insulation model

III. Ground-Wall Insulation Health Monitoring

Historically there have been many methods used to attempt to diagnose insulation problems. The methods most applicable to measuring insulation health on-line measure the leakage current from winding to ground and calculate the impedance of the insulation ground-wall.

Measuring capacitance using residual current was first demonstrated in [22] where phase residual currents were used together with phase-to-phase and phase-to-ground voltages to calculate impedances between each phase and to ground. In [12] residual leakage current is measured via three current sensors, magnetically summing the currents in each phase. In [16], [17] a single current sensor sums the three phase currents together to measure the common mode current at multiples of line frequency. A cheaper method was investigated in [13], [14] using a shunt resistor based current sensor. An alternate method was used in [15] to use the high frequency components of the common mode current to characterize a resonance model to track the change of capacitance over time.

Here, we extend the method presented in [18]. In this method, insulation impedance is measured at inverter drive switching frequencies and multiple harmonics are used. Details are given later in Section IIIB. The method uses multiple harmonics to obtain equivalent R and C. Novelty of the method comes from the method of combining the harmonics into simple parameters resembling standard 50Hz off-line measurement.

Two-level converters use pulse width modulation (PWM) to generate the main line voltage required by the machine. Alongside however, common mode voltages V_{cm}, defined by the sum of the phase voltages to ground in Eq. (2) is also present.

$$V_{cm} = \frac{V_a + V_b + V_c}{3} \quad (2)$$

V_{cm} consists of three sources: a third-harmonic of the mains frequency ($3 \times 50 = 150Hz$) due to the three-phase diode rectifier supplying the DC-link, a third-harmonic of the drive fundamental frequency due to the CM component added in the standard space vector modulation to increase DC-link voltage utilization, and finally the higher frequency components due to the inverter switching.

Fig. 2a shows measured V_{cm} at the terminals of an industrial drive operating at 200Hz fundamental frequency (f_m) with a switching frequency (f_s) of 6 kHz. The frequency spectrum of this signal is shown in Fig. 2c, where the harmonics are clearly identifiable. In Fig. 2c, the first harmonic due to diode rectification is clearly visible at point A at 150Hz; the diode ripple is also observable in the time domain in Fig 2a. The first harmonic of the space vector PWM component is identified in

Fig. 2c as B, at three times the fundamental modulating frequency i.e. 600Hz. The majority of harmonics result from the instantaneous switching voltage and result in harmonics marked by C and D in Fig. 2c, the harmonics at C being at odd multiples of the inverter switching frequency fs and the harmonics at D being sidebands at multiples of f_m, around even multiples of f_s. The common mode voltage constantly acts on the common mode impedance, resulting in a common mode current flowing through the insulation. Measuring this voltage between the winding and ground and leakage current, allows measurement of the insulation impedance.

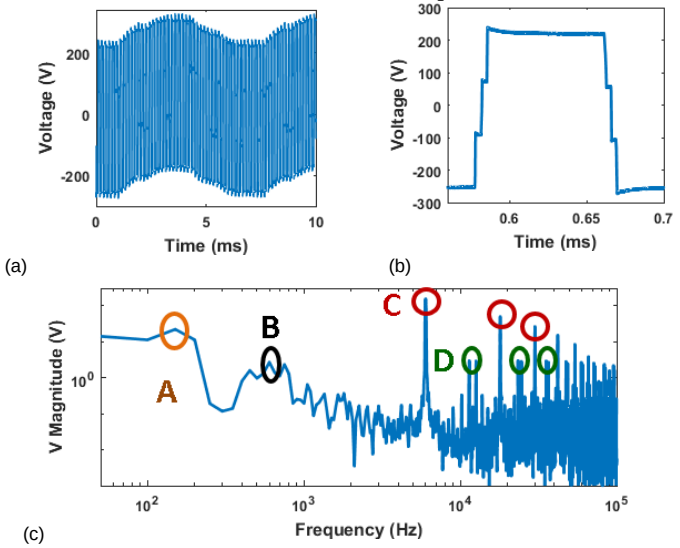

Fig. 2.Common mode voltage (a) time domain, (b) zoomed into a single space vector switching cycle (c) frequency domain

A. *Multi-Frequency Impedance Data*

The off-line and on-line measured equivalent resistances and capacitance for the test machine are shown in Figs. 3 and 4, respectively. The off-line measurement was performed with a Hioki IM3570 impedance analyzer. The resistance decreases steadily from 1kHz to 50kHz because dielectric molecules vibrate faster and dissipate more energy in response to oscillating electric field. At frequencies above 100kHz in this machine, other effects start to dominate. Everything below 50 kHz is therefore designated as "low frequency" for this particular machine.

Measured equivalent capacitance in Fig. 4 indicates that capacitance at low frequencies is constant; however there is an abrupt change at 210 kHz. This is caused by the interaction of the parasitic ground-wall capacitance with the inductances of the winding. The resonance behavior dominates the equivalent R and C values at around 210 kHz. For this paper, only the low frequency results are used.

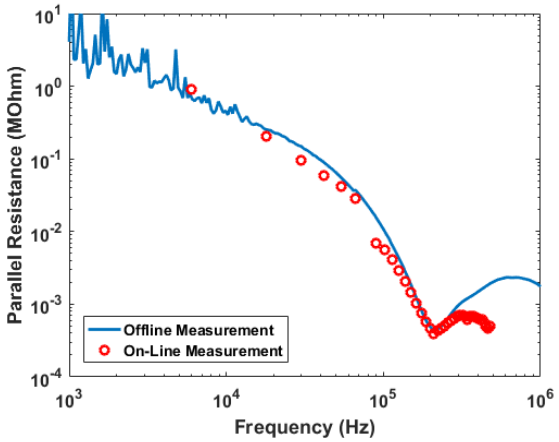

Fig. 3 Equivalent Parallel Resistance of the test machine

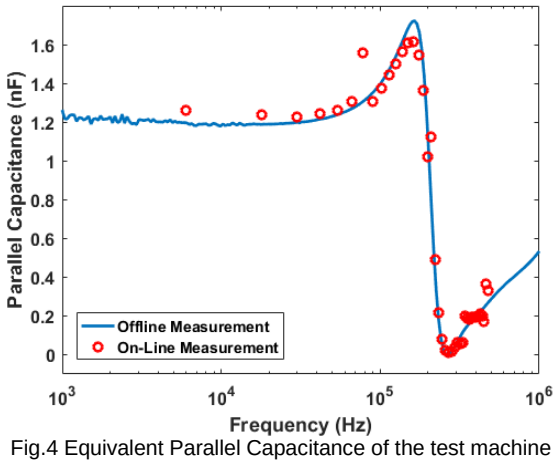

Fig.4 Equivalent Parallel Capacitance of the test machine

The capacitance value in the results section uses an average of the capacitances measured at 6, 18, 30 and 42 kHz. To obtain the result of R_{eq} at 50 Hz, a straight line is fitted to the first four measured harmonics in Fig. 6 and projected to 50Hz. The extrapolated values allow presentation of both the capacitance and dissipation factor at 50Hz to present results in a way more familiar to standard insulation testing. Alternate methods of data presentation and interpretation will be explored by fitting the harmonics to the model in [18] to obtain further information in other publications.

B. *Measurement Equipment and Methodology*

The CM current measurements shown in Fig. 5b, shows that the strongest leakage current harmonic is at the inverter switching frequency f_s. However, leakage current harmonics of similar magnitudes are present into the MHz range.

CM current is measured by summing the phase currents through magnetic cancellation using a high accuracy current transformer. The sensor selected was an ACCT-S-055-MSH closed loop current transformer from Bergoz with a 1MHz bandwidth. For practical industrial applications, it may be possible to relax the sensor bandwidth and sampling requirements to capture only the first few harmonics. V_{cm} is measured here by creating an artificial neutral through a network of resistors. Voltage at the midpoint is the sum of phase voltages, and is measured using a DP-25 differential voltage probe. The experimental setup and the measuring equipment are shown in Fig. 6.

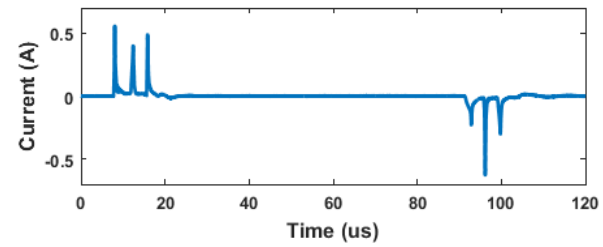

(a)

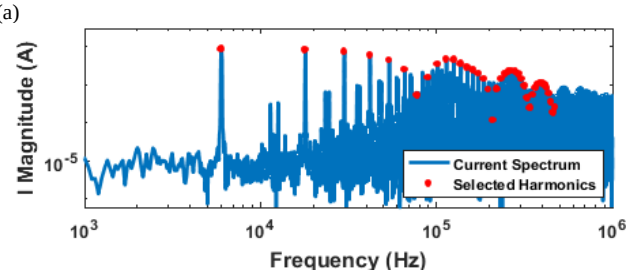

(b)

Fig.5.Measured CM current single cycle (a) and 20ms spectrum (b)

Acquisition and processing of the signals are performed by a Zynq 7010 SoC-based processing board combining an FPGA and an ARM A9 CPU, with two 14-bit 125MS/s analog-to-digital converters (ADC). The data processing chain is summarized in Fig. 7. Data from voltage and current signals acquired by the ADCs enters the FPGA, where it is down-sampled to 25MS/s, filtered and passed to the CPU. The signals are then transferred to the frequency domain using the FFTW3 library by the A9 processor. The first 40 harmonics of the odd multiples of inverter switching frequency, from 6 kHz to 486 kHz are selected. Off-line measured current sensor response is then used to correct the current sensor harmonics. Impedance $Z(\omega)$ of the insulation is calculated in the frequency domain ω by $Z(\omega) = V(\omega)/I(\omega)$ at each frequency. Capacitance and equivalent parallel resistance, representing dissipation, are calculated by applying the parallel RC model in Fig. 1 and calculating the RC values at each frequency using (3)-(4) for capacitance and resistance respectively.

$$C_{eq} = \frac{1}{2\pi f}\frac{1}{|Z|}\sin(-\theta_z) \tag{3}$$

$$R_{eq} = \frac{1}{\frac{1}{|Z|}\cos(\theta_Z)} \tag{4}$$

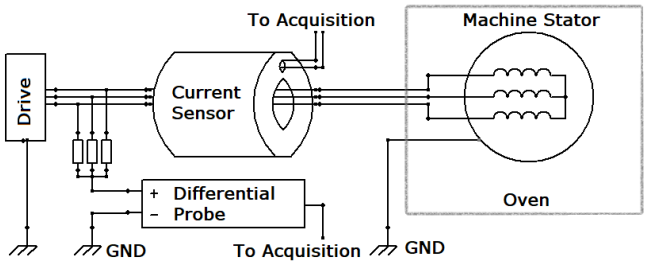

(a)

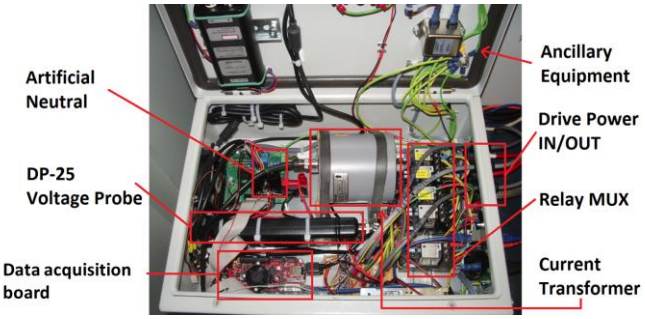

(b)

Fig.6. Experiment equipment setup: schematic (a) and photo (b)

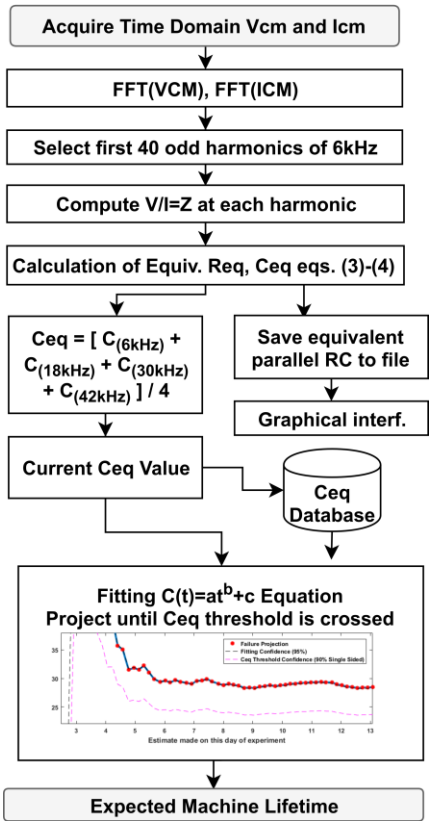

Fig. 7.Data Processing Chain

The impedances are then calculated and stored on-board the system, together with periodic raw voltage and current data for further analysis. For acquisition, 20ms of voltage and current signals are acquired at a time resulting in 2.5 million samples at 125MS/s per channel. Data are downsampled by a factor of 5 inside the FPGA, resulting in 1,000,002 points for both voltage and current. The software is capable of returning the impedance results every 14 seconds. Initial experiments have suggested that a minimum of 10MHz sampling is required to adequately capture the current waveform.

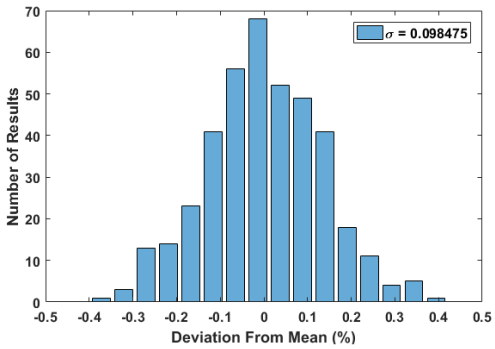

Fig.8 Histogram of measured CM impedance magnitude during 6 hours

The repeatability of the system measurements was evaluated in a preliminary test by running the monitoring system for 6 hours and obtaining 400 impedance magnitude and phase results from a machine operating at room temperature at no load. The distribution of the magnitude results is shown in Fig. 8, where a classic bell curve is observed due to noise. The phase response shows a similar distribution. The standard deviation of the curve in Fig. 8 is less than 0.1%, showing that the system precision is comparable to equipment used in off-line impedance measurement. It is worth noting that these and subsequent tests have been performed at no load with constant fundamental frequency and constant modulation index of 10%. Variation in loading and therefore in the modulation index and fundamental frequency will change the relative magnitudes of some harmonics. However, the frequencies of the dominant harmonics in the CMV, which are at the multiple of the switching frequency, do not change. Since CM voltage and current are directly measured, a change in operating conditions and the resultant change in modulation index does not significantly affect the measurement of the common mode impedance. Results under variable operating conditions will be presented in a forthcoming publication.

IV. Experimental Methodology

Four complete stators of the Unimotor FM 142U2B300VBCAA165240 2.83kW servo motor are used in the experiment for accelerated ageing at four different temperatures. The main aims were to observe the impedance parameters, online, for the first time during ageing with samples operated under PWM conditions representative of real operation. The machine stators are driven by an Emerson M700 drive inverter with a rectified three phase mains input resulting in a 600V DC bus. The inverter applies a rotating voltage space vector to the machine windings, and hence generates a rotating magnetic field inside the stators at 200Hz, operating in open-loop configuration. The rotor is not included with the stators in testing as both the bearings and magnets would be destroyed at the test temperatures before the winding insulation.

Accelerated ageing testing methodology was based on IEEE Std 117 [23], where the insulation temperature is controlled to a constant temperature by the oven test chamber. The machine line voltage was set to 40V due to the absence of back-EMF, and resultant power dissipation in the windings was less than 15W for all samples. The operating frequency and voltage were selected to drive the modulation index above 0.1, representative of normal operation whilst ensuring that internal heating inside the sample was kept to a minimum in order to guarantee uniform temperature distribution. The test sample, together with its high temperature cable can be seen in Fig. 9.

Fig.9 Stator sample inside the temperature controlled chamber

Temperatures of the four samples were selected based on the constraints of time and recommended limits from Std. 117. The four samples operated at 203°C, 215°C, 230°C and 250°C respectively. The samples were deemed as failed when the inverter-drive overcurrent protection circuitry was triggered because of insulation breakdown.

V. Results and Discussion

At the end of test, the cause of sample failure was diagnosed through phase-to-neutral measurements. All samples in this experiment failed through phase-to-phase insulation breakdown. The phase-to-phase insulation in inverter drives is subject to the full DC voltage and it is standard practice to include additional insulation liner between two phases in the end-winding. This particular servomotor omits the extra separation liner as is evident in Fig. 10 to lower manufacturing complexity and cost. The machine used in testing therefore relies on the turn insulation and impregnation in the end-windings for phase-to-phase insulation. During ageing, this insulation degrades and leads to inevitable breakdown.

Fig. 10 Sample 3 End-Windings After Failure. Phase-phase overlap in the EW region is highlighted

While monitoring the ground-wall insulation does not directly measure inter-phase insulation degradation rate, the insulation material and temperatures are the same throughout the machine. The measured trend of ground-wall degradation should therefore be the same as for phase-to-ground.

A. End of Life Times

The temperature index of a material is defined as the temperature that the insulation would be able to maintain a measured physical property for 20,000 hours. In Fig. 10, the sample failure times are plotted against operating temperature

on an Arrhenius plot, with a linear regression fit calculated from the points that extrapolates the lifetime the samples would be expected to have at lower temperatures.

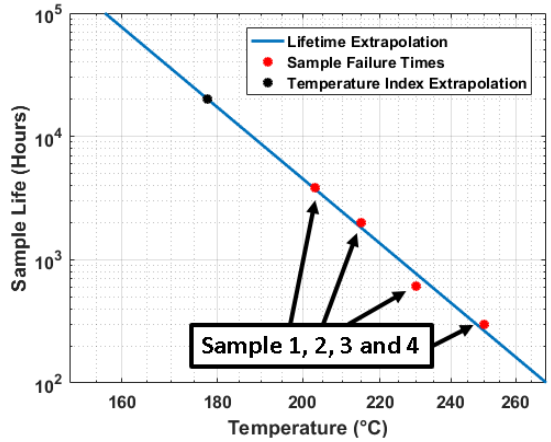

Fig. 11 Arrhenius plot of sample failure times

The measured temperature index of 178 °C, where the fit crosses the 20,000-hour lifetime, compares consistently with the material class rated at 180°C. From this, it can be concluded that the samples as a whole are representative of the material insulation class.

B. Capacitance Results

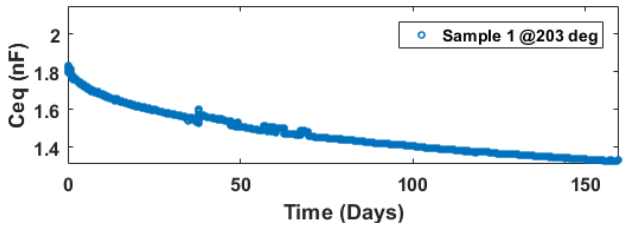

Fig.12 Sample 1 at 203°C C_{eq} plot over time

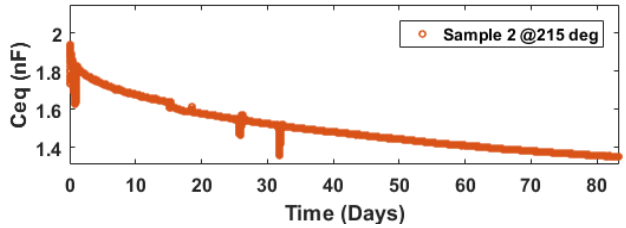

Fig. 13 Sample 2at 215°C C_{eq} plot over time

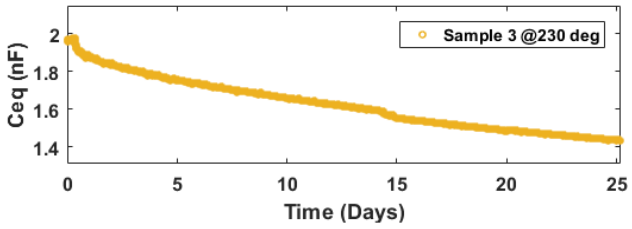

Fig. 14 Sample 3at 230°C C_{eq} plot over time

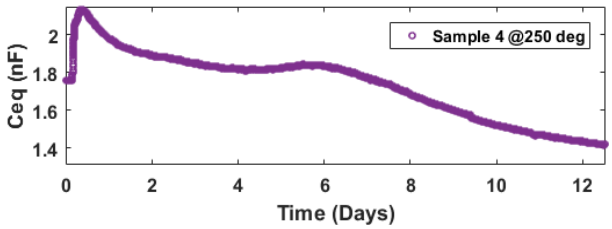

Fig.15 Sample 4at 250°C C_{eq} plot over time

Individual capacitance over time plots for all samples are shown in Figs.12 to 15 in the order of increasing temperature. C_{eq} progression over time decreases for all samples, although Sample 4 shows a temporary increase on day 6 before returning to the decreasing trend. All capacitances decrease in an exponential pattern, the rate of which depends on the test temperature.

Several anomalies are also present and must be noted. In Sample 1, C_{eq} jumps up on day 38. This happened after the experiment was halted due to laboratory relocation. Calibration measurements performed with a high bandwidth impedance analyzer before and after the move rule out equipment malfunction in this measurement. Another interesting jump of C_{eq} occurs in all samples, visible in Sample 1 on day 47 or in Sample 3 on day 14 in Figs 12 and 14, respectively. Sample 2 was driven to full rated current on day 18 during some additional testing. It was found that the sudden capacitance drop on day 15 did not affect the integrity of the winding. All stator samples continued to operate normally after their respective sharp drops of C_{eq}. The full model of insulation in [18] is required to analyze observed anomalies and unexpected movement in capacitance and dissipation data and will be presented in further publications.

C. Dissipation Factor Results

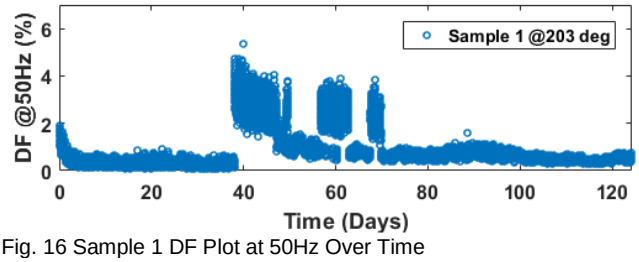

Fig. 16 Sample 1 DF Plot at 50Hz Over Time

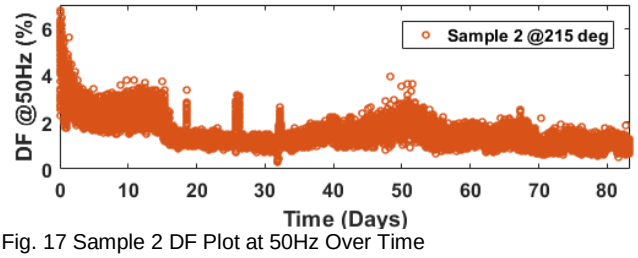

Fig. 17 Sample 2 DF Plot at 50Hz Over Time

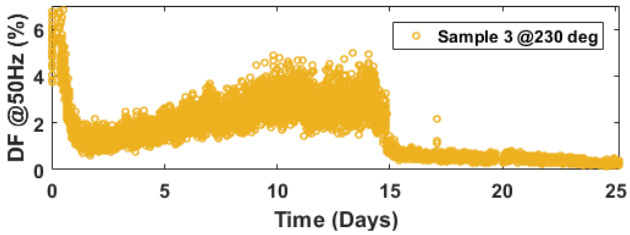

Fig. 18 Sample 3 DF Plot at 50Hz Over Time

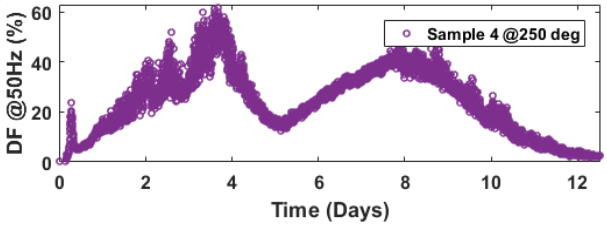

Fig. 19 Sample 4 DF Plot at 50Hz over time

Dissipation results in Figs. 16-19 show a more eventful, less consistent result than the capacitance measurement. The commonalities and differences are noted. The lower temperature samples, 1, 2 and 3 all have similar magnitude of dissipation, between 0.5 to 4%, throughout their lifetime. Sample 4 however has a very high magnitude, as much as 60% equivalent dissipation. The trend of Sample 4 is also a lot more variable, while samples 1, 2 and 3 only have sharp transitions associated with measured capacitance jumps, Sample 4 trend reverses distinctly on day 3, 5 and 8. It is known that oxidation and cross-linking are two competing reactions [21], and it has previously been observed that the balance of these, changes at temperatures around 250°C for class H materials [17]. It is concluded therefore that Sample 4 changed its mode of degradation several times during the course of its lifetime, other samples present variations only relating to change of resonance of the machine. It is recommended to operate at temperatures lower than recommended by test standards to maintain the same ageing mechanism throughout.

VI. Lifetime Prognosis

Initial observations of the C_{eq} results showed a consistent pattern and a relationship with temperature and therefore ageing rate. To compare the results, all capacitance values are plotted in Fig. 20, where C_{eq} values have been normalized to their values at the start of the experiment.

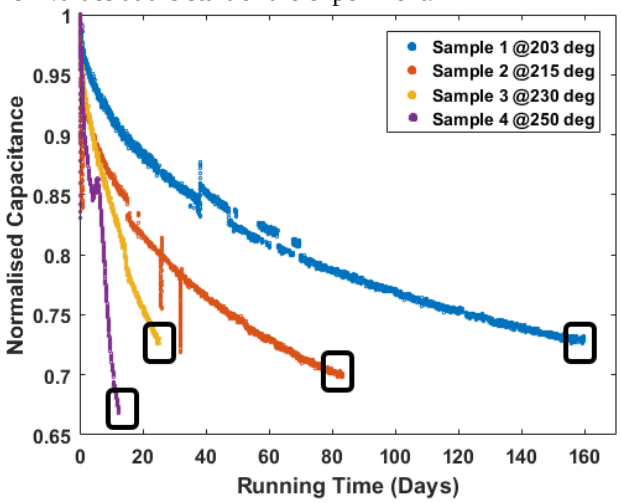

Fig. 20.Normalized C_{eq} over time

In Fig. 20 it can be observed that Samples 1, 2 and 3 failed when the capacitance value reached levels between 69% and 73% of the original value. Sample 4 failed at 66% level. Because it was shown in Fig. 11 that the samples are representative of the population, the final normalized value of capacitance can then be used as a threshold that indicates imminent failure of the insulation system.

To predict the future time of failure, the capacitance data is used as a prognostic tool. Assuming constant temperature, the simple polynomial fit (5) can accurately represent capacitance variation due to thermal ageing as function of time t:

$$C_{eq}(t) = at^b + c \tag{5}$$

In predicting the future in lifetime testing, it is important to consider how representative the samples are of the general population. The effect of confidence boundaries are graphically shown in Figure 21, where two sources of uncertainties are considered: the model parameters fitting confidence boundaries and the final threshold value confidence boundaries. The combined effect of these two is shown in Fig. 21, where the minimum lifetime is shown contrasted with the average lifetime. The zone of uncertainty shows the upper and lower limits of where lifetime of the sample is likely to be.

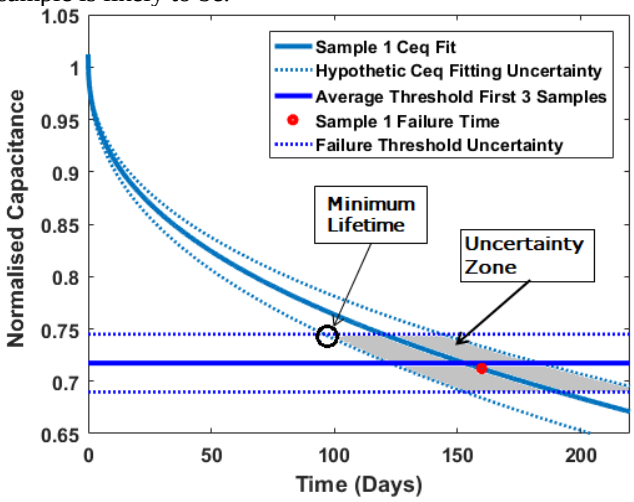

Fig. 21.Fitting of Normalized C_{eq} over time

Fitting capacitance data to (5) can be done using optimization routines e.g. the curve fitting toolbox in MATLAB. These generate the values for coefficients a, b and c as well as the upper and lower limits for each coefficient. Using these limits it is possible to plot the lower and upper deviation of the fit of (5). In Figure 22, the first 6 days' worth of data is used to fit the predicted curve. It can be seen that the fit represents the measured data well, up to day 14 of the experiment, despite using only a fraction of the data in the fit. After the sudden drop in capacitance, the shape continued to be represented well, albeit with an offset. The zoomed in portion of Fig. 22 shows the quality of the fit, the fit performed on day 6 still predicts accurately capacitance data on day 10, with most data falling within the confidence boundaries. It can be concluded that data fitting error is not a significant contributor to the uncertainty of lifetime prediction and that confidence in the final Ceq value must dominate the uncertainty of predicting sample lifetime. Because only three measurements for Ceq value at end of life are available, it is necessary to question, "How representative is the measured value of the general population?" The lifetime for Sample 3 for example is 4.5 days longer than is projected from crossing the threshold at the mean value of 0.717. Confidence thresholds of 90% were selected to calculate when machine failure would occur.

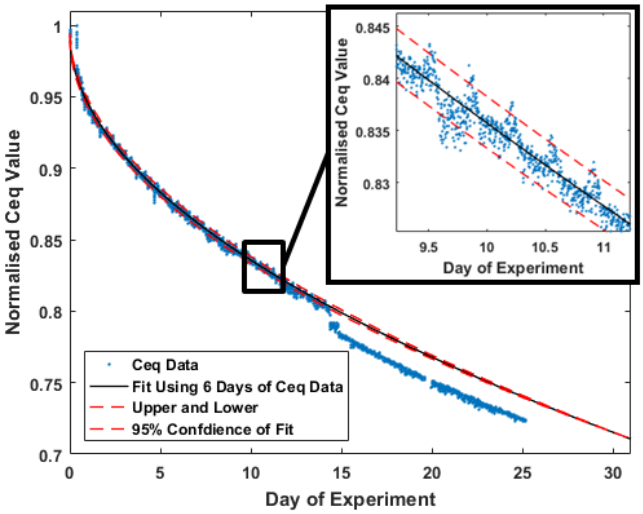

Fig. 22.Fitting of Sample 2 Data

When the value of capacitance for a motor crosses the upper threshold, it should be removed from service due to incipient failure. As we are only interested in when machines start to fail, rather than when most of the machines are likely to have failed, only a single sided confidence value calculation is required. Student t distribution is used to calculate Zi in (6) based on small sample size as per IEEE standard 101 [7]. For the tested samples, the upper limit for the capacitance Ci in (5) is 74.2% of the initial Ceq value.

$$C_i = \bar{x} \pm Z_i \frac{\sigma}{\sqrt{N}} \qquad (6)$$

Fitting of Ceq data has been performed on all samples once a quarter of their lifetime was reached and the fit projected until it reaches both the upper threshold calculated by (6) and the mean value of failure of Ceq at 71.7% of its original value. A summary of the results is shown in Table I where it can be seen that the lifetime estimate for all samples at 90% confidence boundary are less than the final life. Sample 1 would be removed from service on day 128.4; however, 25.7 days of operation would be wasted to guarantee operation. To reduce wastage, it is necessary to either use more samples to establish the mean and the 90% confidence threshold levels or accept a lower level of confidence.

Table I Sample Lifetime Prediction Comparison

	Sample 1	**Sample 2**	**Sample 3**	**Sample 4**
Temperature (°C)	203	215	230	250
C_{eq} reduction (%)	27.2%	30.2%	27.4%	33.2%
Thermal Life Estimate (days)	176.7	83.4	34.3	11.2
Actual Lifetime (Days)	159.8	83.4	25.2	12.5
Fitted Lifetime Prediction (days)	154.1	73.4	28.6	N/A
90% Confidence Lowest Prediction	128.4	59.0	24.7	N/A

VII. On-Line Prognosis

In practice, (5) can be fitted dynamically, with every newly acquired data point. The process of on-line fitting has been implemented on data to predict the sample lifetime of Sample 3 in Fig. 23. The sample lifetime is estimated from the 3rd day up until the 13th, to show the trend of prediction. At first, there is not enough data to make a valid prediction, however with more Ceq data recorded over time, the prediction result starts to converge. Sample lifetime after 5 days' worth of data consistently remains between 28 to 29 days. Both the fitting error and Ceq confidence threshold are plotted alongside to show the range of lifetime that the sample is expected to have. The lowest estimate is 24 days. The sample ended up failing on day 25.6, well within the range of expected values.

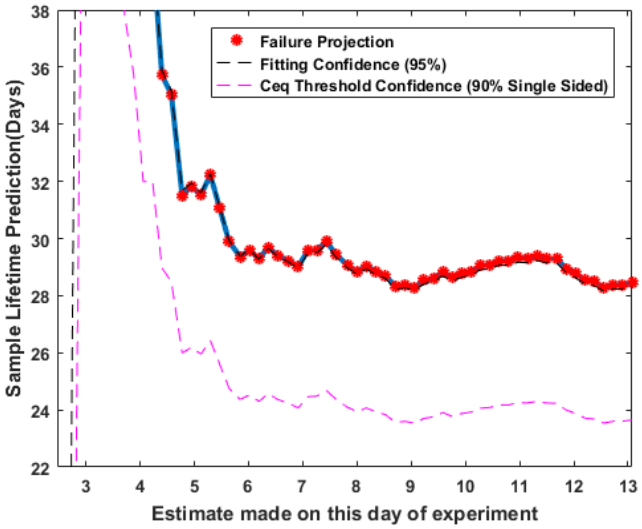

Fig. 23.NormalizedC_{eq} Plot Over Time

VIII. Conclusion

A new method for measuring insulation capacitance and dissipation has been developed and demonstrated on a long-term accelerated ageing experiment of stator insulation. The method, data processing and its application to the online estimation of insulation parameters have been briefly described. The method implements measurement of insulation capacitance with up to 0.1% repeatability while the machine is operating driven by a PWM inverter. The accuracy obtained is similar to that of specialized off-line measurement equipment.

The accelerated ageing methodology of insulation was designed to represent real drive systems as closely as possible. The ageing test was conducted on four stators of low voltage random wound 2.83kW servomotors in a temperature controlled environmental chamber. Accelerated ageing was carried out at four temperatures, to monitor the capacitance and dissipation parameters during ageing and observe resulting trends. The final lifetime of all samples are as expected, returning a temperature index of 178°C for class H material.

It was observed that Sample 4, operating at 250°C, the limit of Class H testing guidelines had a somewhat different ageing profile compared to the other samples. The dissipation data was used to interpret these differences. The other samples had

a consistent C_{eq} trend and final value at end of lifetime, which introduced the idea of fitting the data to extrapolate future time of failure based on C_{eq} data.

The RUL was estimated to demonstrate the fitting and processing to project the end of life. The expected failure times are close to the actual failure times of the machine. Using thresholds from Samples 2 and 4, the RUL was accurately estimated for Sample 1 before failure.

The most important finding during testing was the consistency of capacitance trend over time for all samples and the normalized capacitance value at end of life. It is hoped that through this demonstration, machine manufacturers would record the value of capacitance continuously during internal lifetime validation testing for establishing more certainty in the final threshold value and confidence in the trend across all machines. The proposed method demonstrates a practical and accurate tool for real-time monitoring of insulation health that can be readily employed on high availability machine drives.

A large amount of data has been gathered during the course of this experiment. It was only possible to present a limited number of observations in this paper. A number of events are observable which can be correlated to minor faults or identified as precursor of final deterioration. In-depth analysis of these has been performed using an advanced high frequency insulation model and will be presented in other publications.

The results reported here have been performed in controlled laboratory conditions. Further work is required to validate the proposal in realistic operating conditions.

It is expected that the data presented here and in further publications will contribute to a deeper understanding of the phenomena associated with insulation degradation and contribute novel methods for online prognosis.

REFERENCES

[1] "Report of Large Motor Reliability Survey of Industrial and Commercial Installations, Part I," *IEEE Transactions on Industry Applications*, Vols. IA-21, no. 4, pp. 853-864, 1985.

[2] O. V. Thorsen and M. Dalva, "A Survey of Faults on Induction Motors in Offshore Oil Industry, Petrochemical Industry, Gas Terminals and Oil Refineries," *IEEE Transactions on Industry Applications*, vol. 31, no. 5, pp. 1186-1196, 1995.

[3] Z. Huang, A. Reinap and M. Alaküla, "Degradation and fatigue of epoxy impregnated traction motors due to thermal and thermal induced mechanical stress - part II: Thermal mechanical simulation of multiple wires due to evenly and unevenly distributed temperature," in *8th IET Int. Conf. on Power Electronics, Machines and Drives, Glasgow, PEMD 2016*.

[4] IEC Test Standards, IEC TS 60034-18-41 Standard, International Electrotechnical Commission, 2014.

[5] Culbert, B. Lloyd and G. Stone, "Stator insulation problems caused by variable speed drives," in *Conference Record PCIC Europe*, Barcelona, 2009.

[6] T. W. Dakin, "Electrical Insulation Deterioration Treated as a Chemical Rate Phenomenon," *American Institute of Electrical Engineers, Transactions*, vol. 67, no. 1, pp. 113-122, 1948.

[7] ANSI/IEEE, IEEE Std 101-1987, Guide for the Statistical Analysis of Thermal Life Test Data, 1987, pp. 1-34.

[8] Rusu-Zagar, P. Notingher, V. Navrapescu, G. Mares, G. Rusu-Zagar, T. Setnescu and R. Setnescu, "Method for Estimating the Lifetime of Electric Motors Insulation," in *International Symposium on Advanced Topics in Electrical Engineering*, Bucharest, 2013.

[9] IEEE Std 98-2002, Standard for the Preparation of Test Procedures for the Thermal Evaluation of Solid Electrical Insulating Materials, American National Standard Institute (ANSI), 2002.

[10] Z. Huang, A. Reinap and M. Alaküla, "Dielectric Properties Modeling and Measurement of Single Tooth Coil Insulation System under Accelerated Degradation Test," in *ICEM*, Lausanne, 2016.

[11] K. N. Gyftakis, M. Sumislawska, D. F. Kavanagh, D. A. Howey and M. D. McCulloch, "Dielectric Characteristics of Electric Vehicle Traction Motor Winding Insulation Under Thermal Aging," *IEEE Transactions on Industry Applications*, vol. 52, no. 2, pp. 1398-1404, 2016.

[12] S. B. Lee, J. Yang, K. Younsi and R. M. Bharadwaj, "An online groundwall and phase-to-phase insulation quality assessment technique for AC-machine stator windings," *IEEE Transactions on Industry Applications*, vol. 42, no. 4, pp. 946-957, 2006.

[13] W.R. Jensen, E. Strangas, S. Foster, "A method for online stator insulation prognosis for inverter-driven machines", *IEEE Trans. Industry Applications*, in press. DOI: 10.1109/TIA.2018.2854408

[14] S. Babel and E. G. Strangas, "Condition-based monitoring and prognostic health management of electric machine stator winding insulation," in *International Conference on Electrical Machines (ICEM)*, Berlin, 2014.

[15] P. Nussbaumer, M. A. Vogelsberger and T. M. Wolbank, "Induction Machine Insulation Health State Monitoring Based on Online Switching Transient Exploitation," *IEEE Transactions on Industrial Electronics*, vol. 62, no. 3, pp. 1835-1845, 2015.

[16] K. Younsi, P. Neti, M. Shah, J.Y. Zhou, J. Krahn, K. Weeber, C.D. Whitefield, "On-line capacitance and dissipation factor monitoring of AC stator insulation", I*EEE Trans. On Dielectrics and Electrical Insulation*, vol. 17, n.5, pp. 1441-1452, Oct. 2010

[17] P. Zhang, K. Younsi and P. Neti, "A Novel Online Stator Ground-Wall Insulation Monitoring Scheme for Inverter-Fed AC Motors," in *IEEE Energy Conversion Congress and Exposition (ECCE)*, 2013.

[18] I. Tsyokhla, A. Griffo and J. Wang, "On-line monitoring of winding insulation health using high frequency common mode voltage from PWM," in *IEEE International Electric Machines & Drives Conference (IEMDC*), Coeur d'Alene, ID, 2015.

[19] DuPont Teijin Films, Mylar Polyester Film Electrical Properties (Datasheet H-32192-1), DuPont, 2003.

[20] P. Przybylek and H. Moscicka-Grzesiak, "The Influence of Water Content and Ageing Degree of Paper Insulation on its Mechanical Strength," in *IEEE International Conference on Solid Dielectrics* (ICSD), Potsdam, 2010.

[21] S. Diaham, M.-L. Locatelli and T. Lebey, "Improvement of Polyimide Electrical Properties During Short-Term of Thermal Aging," in *Annual Report Conference on Electrical Insulation and Dielectric Phenomena*, 2008.

[22] G. C. Stone, I. Culbert, E. A. Boulter and H. Dhirani, "Off-Line Rotor and Stator Winding Tests," Ch. 12, in *Rotating Machine Insulation Systems*, in Electrical Insulation for Rotating Machines: Design, Evaluation, Aging, Testing, and Repair, Hoboken, NJ, USA, John Wiley & Sons, Inc, 2014, pp. 235-282.

[23] IEEE Std 117-1974, Test Procedure for Evaluation of Systems of Insulating Materials for Random-Wound AC Electric Machinery, *American National Standard Institute* (ANSI), 1992.

Igor Tsyokhla (M'17), was born in 1991, obtained MEng and PhD degrees in electrical engineering from the University of Sheffield in 2013 and 2017 respectively. After completing his PhD in the field of electrical machine health and condition monitoring, he worked as Research Associate with the University of Sheffield developing condition monitoring hardware and developing models for lifetime prognostics. He has a broad interest in all areas of electrical engineering, his specialities include insulation monitoring, automation and machine reliability. Dr Tsyokhla is currently working in industry to develop automated biological cell sorting technology using microfluidics, fluorescence and computer vision.

Antonio Griffo (M'13) received the M.Sc. degree in electronic engineering and the Ph.D. degree in electrical engineering from the University of Napoli "Federico II," Naples, Italy, in 2003 and 2007, respectively. From 2007 to 2013, he was a Research Associate with The University of Sheffield, Sheffield, U.K., and the University of Bristol, Bristol, U.K. He is currently a Senior Lecturer in the Department of Electronic and Electrical Engineering, The University of Sheffield. His research interests include modeling, control, and condition monitoring of electric power systems, power electronics converters, and electrical motor drives for renewable energy, automotive, and aerospace applications.

Jiabin Wang (SM'03) received the B.Eng. and M.Eng. degrees from Jiangsu University, Zhenjiang, China, in 1982 and 1986, respectively, and the Ph.D. degree from the University of East London, London, U.K., in 1996, all in electrical and electronic engineering. He is currently a Professor of electrical engineering at The University of Sheffield, Sheffield, U.K. From 1986 to 1991, he was with the Department of Electrical Engineering, Jiangsu University, where he was appointed a Lecturer in 1987 and an Associate Professor in 1990. He was a Postdoctoral Research Associate at The University of Sheffield from 1996 to 1997 and a Senior Lecturer at the University of East London from 1998 to 2001. His research interests range from motion control and electromechanical energy conversion to electric drives for applications in automotive, renewable energy, household appliances, and aerospace sectors.

Dr. Wang is a Fellow of the Institution of Engineering and Technology, U.K